

Quantum simulation of non-Markovianity using the quantum Zeno effect

Sabrina Patsch,¹ Sabrina Maniscalco,^{2,3} and Christiane P. Koch¹

¹*Theoretische Physik, Universität Kassel, Heinrich-Plett-Straße 40, D-34132 Kassel, Germany*

²*QTF Centre of Excellence, Turku Centre for Quantum Physics,*

Department of Physics and Astronomy, University of Turku, FIN-20014 Turku, Finland

³*QTF Centre of Excellence, Department of Applied Physics, Aalto University, FIN-00076 Aalto, Finland*

(Dated: March 21, 2022)

We suggest a quantum simulator that allows to study the role of memory effects in the dynamics of open quantum systems. Our proposal is based on a bipartite quantum system consisting, for simplicity, of a harmonic oscillator and a few-level system; it exploits the formal analogy between dissipation and quantum measurements. The interaction between the subsystems gives rise to quantum Zeno dynamics, and the dissipation strength experienced by the harmonic oscillator can be tuned by changing the parameters of the measurement, i.e., the interaction with the few-level system. Extension of the proposal to anharmonic systems is straightforward.

Quantum simulation uses a controllable quantum system to study another less controllable quantum system [1]. It promises to advance the study of many-body dynamics in condensed matter physics [1], but application to open quantum systems is also most natural [2–17]. Quantum simulation of open quantum system dynamics can be based on algorithmic methods [7–9, 11], stochastic Hamiltonians [12] and Hamiltonian ensembles [15], or stochastic quantum walks [13]. Experimental realizations to date have focussed on qubit dynamics, encoding the system in trapped ions [3], photon polarization [4, 6, 16, 17] and nuclear spins [10], but more complex systems such as the light harvesting complex have also been suggested [5]. A key interest in the quantum simulation of open quantum systems is the controllable transition from Markovian to non-Markovian dynamics. It implies the ability to study memory effects and is motivated in a two-fold way. First, non-Markovian dynamics are ubiquitous in condensed phase [18], encountered in settings as different as light harvesting or solid-state based quantum technologies, but inherently difficult to describe and study [19]. Second, memory effects may present a resource that can be exploited [20, 21]. For example, non-Markovian dynamics were shown to allow for more efficient cooling [22], better quantum communication [23, 24], and improved quantum gate operation [25, 26]. The different physical aspects underlying these improvements are captured by the various measures to quantify non-Markovianity [27, 28]. The transition from Markovian to non-Markovian dynamics is comparatively easy to achieve when system and environmental degrees are carried by the same physical object, for example the polarization and frequency of a photon [4, 16]. However, for a multi-partite implementation of the open system simulator one needs to engineer suitable environmental correlations or a sufficiently strong interaction between system and environment for memory effects to come into play. The latter has been realized by implementing the simulated interaction between system and environment by quantum circuits [10], whereas the for-

mer is possible when using controllable systems to represent the environment, such as quantum inductor-resistor-capacitor oscillators in a superconducting qubit architecture [5].

Here, we provide a general framework for inducing and tailoring essentially arbitrary open system dynamics based on quantum measurements. To this end, the system is coupled to a meter which is measured destructively.

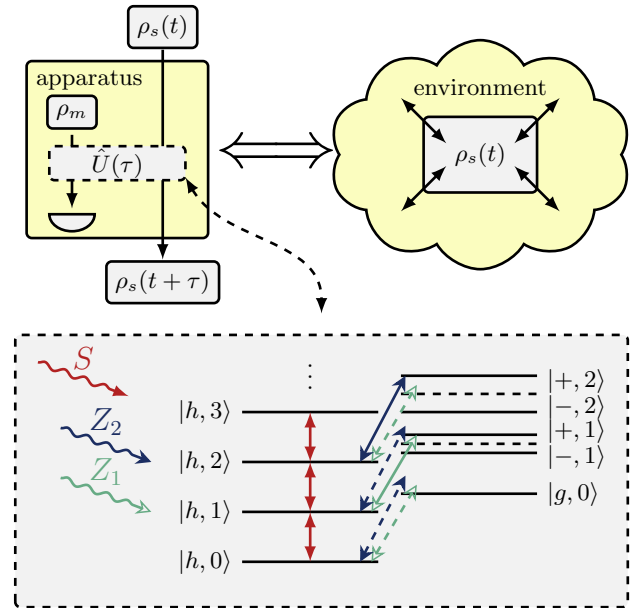


FIG. 1. (Color online) Analogy between the indirect measurement of a system ρ_s using a meter ρ_m (top left) and an open quantum system (top right). Bottom: Energy level diagram of a bipartite system consisting of a harmonic oscillator and a few-level system, interacting with three external fields—the drive S of the harmonic oscillator (red), and two Zeno pulses $Z_{z=1}$ (green, open notched arrowhead) and $Z_{z=2}$ (blue, notched arrowhead) addressing the levels $|z = 1\rangle$ and $|z = 2\rangle$. Arrows with solid (dashed) lines indicate resonant (off-resonant) transitions.

tively after a short interaction time, cf. Fig. 1 (top). In the limit of quasi-continuous measurements, this leads to confinement of the systems dynamics to a specific subspace, i.e., to quantum Zeno dynamics [29]. We show here that the control available in the measurement process can be used to tune the system dynamics from being memory-less to exhibiting effects of memory.

Theoretical framework — For simplicity, we take the system that is connected to a tunable source of dissipation to be a harmonic oscillator (HO), $\hat{H}_s = \sum_n \omega n |n\rangle \langle n|$, where we have set the vacuum energy to zero ($\hbar = 1$ throughout). It would also be possible to assume a finite n -level system instead for achieving qualitatively the same results. The system is coupled to a meter which we model by a three-level system with states $|g\rangle$, $|e\rangle$, and $|h\rangle$, $\hat{H}_m = \omega' |g\rangle \langle g| + (\omega + \omega') |e\rangle \langle e|$. The energy of $|h\rangle$ is set to zero and the $|g\rangle \leftrightarrow |e\rangle$ transition is resonant with the HO transition frequency ω while the $|h\rangle \leftrightarrow |g\rangle$ transition is far off-resonant with $\omega \ll \omega'$. The meter can easily consist of more than three levels but existence of one resonant and at least one off-resonant transition is essential. The resulting coupling, in the interaction picture with respect to the drift Hamiltonian, $\hat{H}_0 = \hat{H}_s + \hat{H}_m$, and using the rotating wave approximation, can then be described by a Jaynes-Cummings type interaction [30],

$$\hat{H}_{sm} = \frac{\Omega}{2} (\hat{\sigma}_- \hat{a}^\dagger + \hat{\sigma}_+ \hat{a}) \quad (1)$$

with Rabi frequency Ω , $\hat{\sigma}_- = |g\rangle \langle e| = \hat{\sigma}_+^\dagger$, and creation and annihilation operators $\hat{a}^{(\dagger)}$ for the HO. The eigenstates of \hat{H}_{sm} are the dressed states $|g, 0\rangle$, and $|\pm, n\rangle = \frac{1}{\sqrt{2}} (|e, n-1\rangle \pm |g, n\rangle)$ for $n \geq 1$ with eigenenergies $E_n^\pm = \omega n \pm \frac{\Omega}{2} \sqrt{n}$ [30], cf. Fig. 1 (bottom). In addition to its coupling to the meter, the HO is driven by a resonant classical source S with field strength α ,

$$\hat{H}_S = \alpha \hat{a}^\dagger + \alpha^* \hat{a}. \quad (2)$$

We assume the drive to be weak compared to the coupling with the meter, $\alpha \ll \Omega$, such that the HO will only be driven if the meter is in $|h\rangle$. In this limit, \hat{H}_S will induce a displacement $\beta = -i\alpha\tau$ of the HO's state, $\hat{U}_S(\tau) = e^{-i\hat{H}_S\tau} = e^{\beta\hat{a}^\dagger - \beta^*\hat{a}}$.

A tunable source of dissipation is introduced by a series of indirect measurements of the HO's state using identical meters, cf. Fig. 1 (top). These measurements shall determine whether the HO is in a specific Fock state $|z\rangle$, the 'Zeno level'. To this end, HO and meter are coupled by a so-called Zeno pulse Z_z with coupling strength ω_z which is resonant to the $|h, z\rangle \leftrightarrow |+, z\rangle$ transition,

$$\hat{H}_z = \frac{\omega_z}{2} \left(|h, z\rangle \langle +, z| + |+, z\rangle \langle h, z| \right), \quad (3)$$

cf. Fig. 1 (bottom). If and only if the HO is in the Zeno level, Z_z will induce Rabi oscillations, $\hat{U}_z(\tau) =$

$e^{-i\hat{H}_z\tau} = e^{(|h, z\rangle \langle +, z| + |+, z\rangle \langle h, z|) \phi_z / 2}$, accumulating a Rabi angle $\phi_z = \omega_z\tau$ during the interaction time τ . Thus, there will only be population in the state $|+, z\rangle$ if there was population in $|z\rangle$ initially. A subsequent destructive measurement of the meter at time τ , corresponding to a partial trace over the meter, thus provides information on the population of $|z\rangle$ [29]. The state of the HO at the end of one time interval τ can be obtained in terms of piecewise dynamics,

$$\hat{\rho}_s(t + \tau) = \text{Tr}_m \left\{ \hat{U}(\tau) \hat{\rho}(t) \hat{U}^\dagger(\tau) \right\} \quad (4)$$

with $\hat{U}(\tau) = e^{-i(\hat{H}_S + \hat{H}_{sm} + \hat{H}_z)\tau}$ and $\hat{\rho}$ ($\hat{\rho}_s$) denoting the density operator of the bipartite system (the HO). The procedure of coupling the HO to a meter during time τ and performing a destructive measurement of the meter afterwards is repeated several times, with the new meter initially always in $|h\rangle$. For small displacements, $|\beta| \ll 1$, of the HO in between two measurements, the protocol gives rise to quantum Zeno dynamics (QZD) [29, 31, 32]. Hence, when choosing an initial state of the system below the Zeno level, $|n_0 < z\rangle$, the dynamics is confined to the Zeno subspace $\mathcal{H}_Z^< = \{|0\rangle, \dots, |z-1\rangle\}$. The displacement β , due to the drive S , and the Rabi angle ϕ_z , due to the Zeno pulse Z_z , act as "knobs" to control the dynamics of the quantum simulator as we show below.

The proposed scheme can be realized experimentally in several ways. In cavity or circuit QED, the HO corresponds to a cavity mode while three neighboring circular states of a Rydberg atom flying through the cavity [29] or a superconducting qubit coupled to the cavity [33] encode the three-level system. The example of a cavity QED implementation is discussed in more detail in the Supplemental Material (SM) [34]. Similarly, a common vibrational mode of trapped ions together with ion qubit states also realize the envisioned bipartite system [35]. However, the system does not need to be harmonic for the model to work. The model is even more general since the system does not have to be bipartite—it is sufficient to identify two different subspaces in the quantum system: a 'system' and a 'meter' part and carry out a state-selective measurement of the 'system' using the 'meter'. An example for a unary realization would be a Bose-Einstein condensate (BEC) with hyperfine ground state levels encoding the system [36]. In this case, the open quantum system is matter-based, instead of photonic as in the cavity or circuit QED setup. In general, realization of our proposal requires three conditions to be met: (i) existence of a 'system' part whose dynamics are decoupled from the 'meter' part when driven by a source S , (ii) selective excitation of system states by driving transitions in the meter using the Zeno pulse Z_z , (iii) subjecting meter states to dissipation. Dissipation can be introduced by projective measurement of the meter, or it can be natural such as a fast decay. In the BEC example, the Zeno pulse drives transitions to an excited state hyperfine ma-

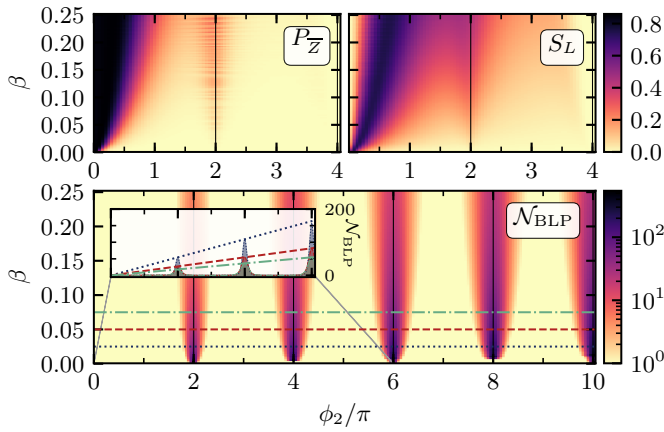


FIG. 2. (Color online) Infidelity $P_{\bar{Z}}$ of the quantum Zeno dynamics, dissipation S_L , and non-Markovianity measure \mathcal{N}_{BLP} as a function of the displacement β due to the classical drive S and the Rabi angle ϕ_2 accumulated due to the Zeno pulse Z_2 . Inset: \mathcal{N}_{BLP} as a function of ϕ_2 for $\beta = 0.025$ (blue dotted, highest peaks), 0.050 (red dashed) and 0.075 (green dash-dotted, smallest peaks) with linearly increasing peak heights.

nifold [36] such that the meter is subject to spontaneous decay.

Simulating an open quantum system — To illustrate the implementation of the simulator, we choose the overall protocol duration such that $-i\alpha T = 2\pi$, take the initial state to be $|n_0 = 0\rangle$ and the Zeno level $|z = 2\rangle$ such that QZD occurs in the two-dimensional Zeno subspace $\mathcal{H}_Z = \{|0\rangle, |1\rangle\}$. To quantify the amount of dissipation, we use the linear entropy, $S_L = 1 - \text{Tr}\{\hat{\rho}^2\}$; and the population $P_{\bar{Z}}$ that has escaped from the Zeno subspace \mathcal{H}_Z , $P_{\bar{Z}} = \sum_{n=2}^{\infty} \langle n | \hat{\rho}_s(T) | n \rangle$, measures the QZD infidelity.

We expect the system dynamics to display memory effects and use the so-called BLP measure quantifying non-

Markovianity as accumulated revivals in distinguishability of two initial states [37]. The optimal state pair which maximizes the BLP measure for our choice of α and $|z\rangle$ is given by

$$|\Psi_1(\vartheta)\rangle = \cos\left(\frac{\vartheta}{2}\right)|0\rangle + \sin\left(\frac{\vartheta}{2}\right)|1\rangle, \quad |\Psi_2\rangle = |2\rangle \quad (5)$$

for all $\vartheta \in [0, 2\pi)$ [34], and we take $\vartheta = 0$ in the following.

We start by discussing the quantum simulator subject to the classical drive S and only one Zeno pulse with Zeno level $|z = 2\rangle$, cf. Fig. 2. An arbitrary degree of dissipation, as indicated by S_L , can be engineered by tuning the displacement β induced by the classical drive and the Rabi angle $\phi_{z=2}$ due to the Zeno pulse. More specifically, large dissipation can be realized by choosing a small ϕ_2 while strong non-Markovianity can be engineered by setting ϕ_2 to multiples of 2π . Dissipation occurs mostly in the parameter range where the population leaves the Zeno subspace [34], except for $\phi_2 \rightarrow 0$, where no dissipation occurs since the coupling of system and meter vanishes. Both the infidelity of the QZD and the dissipation are vanishingly small for Rabi angles $\phi_2 > 4\pi$ [34] which is why this parameter range is omitted from Fig. 2.

The signatures of non-Markovianity are strongest for Rabi angles $\phi_2 = 2n\pi$ with n being an integer, cf. Fig. 2 (bottom). This is because a pulse Z_z with $\phi_z = 2n\pi$ corresponds to the map $|h, z\rangle \mapsto (-1)^n |h, z\rangle$ after the time interval τ , i.e., the pulse changes only the phase of the Zeno level and no entanglement between system and meter is left [38]. For other Rabi angles, $\phi_z \neq 2n\pi$, entanglement remains between system and meter at the end of the time interval τ . Measurement of the meter then erases information, resulting in less distinguishable states in \mathcal{N}_{BLP} and the system dynamics becoming Markovian. In the Markovian limit, the dynamics can be described by a master equation of Lindblad form by assuming quasi-continuous measurements [34],

$$\frac{d\hat{\rho}_s(t)}{dt} = -i \left[\hat{H}_S, \hat{\rho}_s(t) \right] + \kappa\gamma_A \left(\hat{A}\hat{\rho}_s(t)\hat{A}^\dagger - \frac{1}{2} \left\{ \hat{A}^\dagger\hat{A}, \hat{\rho}_s(t) \right\} \right) + \kappa\gamma_\Pi \left(\hat{\Pi}\hat{\rho}_s(t)\hat{\Pi}^\dagger - \frac{1}{2} \left\{ \hat{\Pi}^\dagger\hat{\Pi}, \hat{\rho}_s(t) \right\} \right) \quad (6)$$

with $\kappa = 1/\tau$, $\hat{\Pi} = |z\rangle\langle z|$ and $\hat{A} = |z-1\rangle\langle z|$, and

$$\gamma_A = \frac{1}{2} \sin^2 \frac{\phi_z}{2}, \quad \gamma_\Pi^* = 2 \sin^2 \frac{\phi_z}{4}, \quad \gamma_\Pi = \gamma_\Pi^{*2} + \gamma_A. \quad (7)$$

Given the definitions of \hat{A} and $\hat{\Pi}$, $\kappa\gamma_A$ corresponds to the rate of population transfer from the Zeno level to the level below, and $\kappa\gamma_\Pi$ to the dephasing rate of the Zeno level. The master equation provides yet another angle illustrating the functionality of the quantum simulator, in addition to Fig. 2: The decay rates can be varied by tuning the experimentally accessible parameters ϕ_z and

κ . In the non-Markovian regime ($\phi_2 \simeq 2n\pi$) and for a given displacement β , the value of the non-Markovianity measure increases approximately linearly with the Rabi angle ϕ_2 (see inset in Fig. 2). For constant ϕ_2 in turn, the non-Markovianity measure decreases as β gets larger since it is inversely proportional to the Zeno pulse field strength $\omega_Z = \phi_2/\tau \propto \phi_2/\beta$. However, with only a single Zeno pulse, dissipation and memory effects cannot be tuned independently.

This can be remedied by employing two state-selective excitations simultaneously, cf. Fig. 1. Specifically, we as-

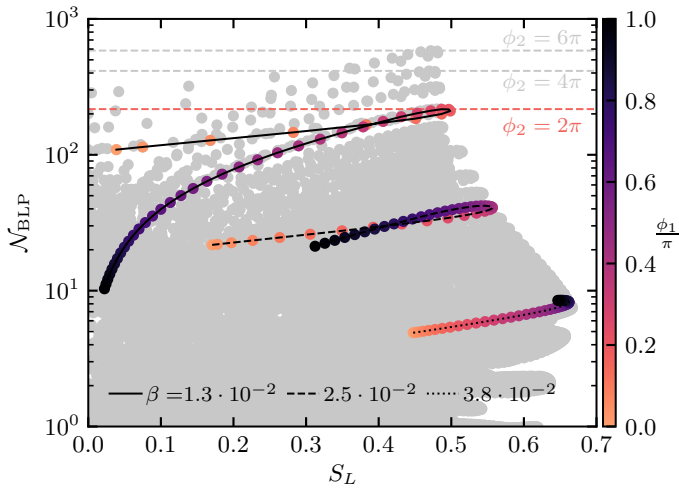


FIG. 3. (Color online) Attainable combinations of dissipation S_L and non-Markovianity \mathcal{N}_{BLP} using two Zeno pulses Z_2 and Z_1 (grey dots) with the colored dots highlighting the combinations for a Rabi angle $\phi_2 = 2\pi$ and three different values of β . The color of the dots encodes the value of the Rabi angle ϕ_1 as indicated by the color bar, and lines connect the dots with the same value of the displacement β as given by the line style. The horizontal dashed lines indicate the maximal value of \mathcal{N}_{BLP} when tuning ϕ_2 to 2π , 4π and 6π .

sume state-selective excitation of the Fock state $|2\rangle$ by the Zeno pulse Z_2 and of $|1\rangle$ by another Zeno pulse Z_1 (for a system with a larger Hilbert space, any two distinct levels can be chosen). While Z_2 controls memory effects, Z_1 induces dissipation. Large memory effects require a Rabi angle ϕ_2 close to multiples of 2π , whereas small ϕ_1 , i.e., ϕ_1 smaller than π for our values of the displacement β , results in strong dissipation. Note that, despite employing two Zeno fields, still only a single measurement needs to be carried out at the end of each time interval τ . Fig. 3 shows that any combination of dissipation strength, quantified by the linear entropy S_L , and memory effects, quantified by the measure \mathcal{N}_{BLP} (calculated with $\vartheta = \pi$ [34]), can be attained by varying the displacement β and the two Rabi angles ϕ_2 and ϕ_1 . The gray dots in Fig. 3 show all combinations of S_L and \mathcal{N}_{BLP} obtained by sampling β from $1.26 \cdot 10^{-2}$ to 0.251 in 20 steps, ϕ_2 from 0 to 6π in steps of 0.1π and ϕ_1 from 0 to π in steps of 0.025π . In order to illustrate how the change in one of the three parameters affects the dissipation strength and memory effects, we inspect the special case $\phi_2 = 2\pi$ for three different values of β , represented by different lines, and varying ϕ_1 , as encoded in the color bar in Fig. 3. When considering, for instance, the points on the solid line, corresponding to the smallest considered value of β , an increase of the Rabi angle ϕ_1 (moving from the lightest point on the upper left end to the right) leads to a large increase of dissipation but initially only to a small increase degree in the non-Markovianity measure. When ϕ_1 takes the value 0.175π , the line reaches

a turning point where the dissipation takes its maximal value with $S_L = 0.5$. A further increase in ϕ_1 results in a decrease of both dissipation and non-Markovianity measure. This is because the pulse Z_1 starts to build up a Zeno barrier at $|1\rangle$ which prevents dissipation. For larger β , cf. the dashed and dotted lines, the dissipation becomes stronger, and a larger value of ϕ_1 is needed to build up a Zeno barrier. Accordingly, the turning point of these lines is shifted to larger values of S_L and ϕ_1 . The picture is very similar for larger Rabi angles $\phi_2 = 2n\pi$ but the maximally attainable degree of non-Markovianity increases, as indicated by the dashed horizontal lines in Fig. 3. When ϕ_2 takes values inbetween multiples of 2π , the non-Markovian measure decreases quickly which allows to realize dynamics without memory effects. Since, in an experiment, the three parameters β , ϕ_2 and ϕ_1 can be tuned essentially continuously, the areas inbetween the gray dots can also be attained.

While we have restricted our analysis here to a two-dimensional subspace of the system's Hilbert space, generalization to larger subspaces is straightforward. Indeed, to create a subspace with dimension z_0 , one simply needs to choose the Zeno level $|z_0\rangle$, i.e., adjust the frequency of the Zeno pulse Z_{z_0} , accordingly. The dimension of the system should therefore at least be three in order to enable non-trivial dynamics, but can be arbitrarily large and even infinite as in the cavity QED application [29]. Moreover, it is also possible to generate dissipation and memory effects on multiple system states $|z_i\rangle$ with $i \in \{1, 2, \dots, N\}$ by varying the frequency of the Zeno pulse Z_{z_0} as a function of time or by employing multiple Zeno pulses Z_{z_i} and tailoring the Rabi angles as explained above. The number N of maximally controllable states is then limited by the dimension of the 'meter' subspace. In a cavity or circuit QED setup, this subspace is formed by the dressed states and is thus infinite. In the BEC experiment [36], the limit is given by the size of the second hyperfine manifold.

Conclusions — We have introduced a quantum simulator for open quantum system dynamics based on a series of indirect, state-selective measurements of a system by a meter. The driven system dynamics becomes open when tracing out the meter, i.e., our proposal relies on the formal analogy between measurement and dissipation. The open system dynamics can be tuned from memory-less to displaying maximal memory effects by choosing the amount of entanglement between system and meter at the end of their interaction. This represents a direct realization of memory effects in terms of repeated interactions between system and environment and past-future independence [39]. The amount of dissipation and the degree of non-Markovianity can be engineered independently by a suitable choice of the amplitudes of a classical drive for the system and two Zeno pulses probing the system states dressed by the interaction with the meter, whereas the frequency of the Zeno pulses determines

which system levels are subject to dissipation. Our proposal opens the way to experimentally realize quantum simulation of open quantum systems, studying memory effects in a controlled way. This would allow, for example, to clarify the role of memory effects for the controllability of an open quantum system [40] and address the question whether and how memory effects alter control strategies for open quantum systems.

We thank J.-M. Raimond, S. Gleyzes, F. Assémat, and E. M. Laine for discussions. Financial support from the European Union under the Research and Innovation action project “RYSQ” (Project No. 640378), the DAAD/Academy of Finland mobility grants, and the Studienstiftung des deutschen Volkes e.V. is gratefully acknowledged. This work was partly done using the high-performance computing cluster FUCHS-CSC provided by the Center for Scientific Computing (CSC) of the Goethe University Frankfurt in the framework of the HHLR-GU (Hessisches Hochleistungsrechenzentrum der Goethe-Universität).

-
- [1] I. M. Georgescu, S. Ashhab, and F. Nori, *Rev. Mod. Phys.* **86**, 153 (2014).
- [2] S. Maniscalco, J. Piilo, F. Petruccione, and A. Messina, *Acta Physica Hungarica Series B, Quantum Electronics* **23**, 67 (2005).
- [3] J. T. Barreiro, M. Müller, P. Schindler, D. Nigg, T. Monz, M. Chwalla, M. Hennrich, C. F. Roos, P. Zoller, and R. Blatt, *Nature* **470**, 486 (2011).
- [4] B.-H. Liu, L. Li, Y.-F. Huang, C.-F. Li, G.-C. Guo, E.-M. Laine, H.-P. Breuer, and J. Piilo, *Nature Phys.* **7**, 931 (2011).
- [5] S. Mostame, P. Rebentrost, A. Eisfeld, A. J. Kerman, D. I. Tsomokos, and A. Aspuru-Guzik, *New J. Phys.* **14**, 105013 (2012).
- [6] A. Chiuri, C. Greganti, L. Mazzola, M. Paternostro, and P. Mataloni, *Sci. Rep.* **2**, 968 (2012).
- [7] R. Sweke, I. Sinayskiy, and F. Petruccione, *Phys. Rev. A* **90**, 022331 (2014).
- [8] R. Sweke, I. Sinayskiy, D. Bernard, and F. Petruccione, *Phys. Rev. A* **91**, 062308 (2015).
- [9] R. Sweke, M. Sanz, I. Sinayskiy, F. Petruccione, and E. Solano, *Phys. Rev. A* **94**, 022317 (2016).
- [10] N. K. Bernardes, J. P. S. Peterson, R. S. Sarthour, A. M. Souza, C. H. Monken, I. Roditi, I. S. Oliveira, and M. F. Santos, *Sci. Rep.* **6**, 33945 (2016).
- [11] U. Alvarez-Rodriguez, R. Di Candia, J. Casanova, M. Sanz, and E. Solano, *Phys. Rev. A* **95**, 020301 (2017).
- [12] A. Chenu, M. Beau, J. Cao, and A. del Campo, *Phys. Rev. Lett.* **118**, 140403 (2017).
- [13] L. C. G. Govia, B. G. Taketani, P. K. Schuhmacher, and F. K. Wilhelm, *Quantum Sci. Technol.* **2**, 015002 (2017).
- [14] E. Mascarenhas and I. de Vega, *Phys. Rev. A* **96**, 062117 (2017).
- [15] H.-B. Chen, C. Gneiting, P.-Y. Lo, Y.-N. Chen, and F. Nori, *Phys. Rev. Lett.* **120**, 030403 (2018).
- [16] Z.-D. Liu, H. Lyyra, Y.-N. Sun, B.-H. Liu, C.-F. Li, G.-C. Guo, S. Maniscalco, and J. Piilo, *Nature Commun.* **9**, 3453 (2018).
- [17] Ivaro Cuevas, A. Gherardi, C. Liorni, L. D. Bonavena, A. D. Pasquale, F. Sciarrino, V. Giovannetti, and P. Mataloni, *Sci. Rep.* **9**, 3205 (2019).
- [18] U. Weiss, *Quantum dissipative systems*, 4th ed. (World Scientific, 2012).
- [19] I. de Vega and D. Alonso, *Rev. Mod. Phys.* **89**, 015001 (2017).
- [20] K.-D. Wu, Z. Hou, G.-Y. Xiang, C.-F. Li, G.-C. Guo, D. Dong, and F. Nori, arXiv:1903.03359 (2019).
- [21] N. Anand and T. A. Brun, arXiv:1903.03880 (2019).
- [22] R. Schmidt, A. Negretti, J. Ankerhold, T. Calarco, and J. T. Stockburger, *Phys. Rev. Lett.* **107**, 130404 (2011).
- [23] E.-M. Laine, H.-P. Breuer, and J. Piilo, *Sci. Rep.* **4**, 4620 (2014).
- [24] B. Bylicka, D. Chruściński, and S. Maniscalco, *Sci. Rep.* **4**, 5720 (2014).
- [25] P. Rebentrost, I. Serban, T. Schulte-Herbrüggen, and F. K. Wilhelm, *Phys. Rev. Lett.* **102**, 090401 (2009).
- [26] D. M. Reich, N. Katz, and C. P. Koch, *Sci. Rep.* **5**, 12430 (2015).
- [27] Á. Rivas, S. F. Huelga, and M. B. Plenio, *Rep. Prog. Phys.* **77**, 094001 (2014).
- [28] H.-P. Breuer, E.-M. Laine, J. Piilo, and B. Vacchini, *Rev. Mod. Phys.* **88**, 021002 (2016).
- [29] J. M. Raimond, P. Facchi, B. Peaudecerf, S. Pascazio, C. Sayrin, I. Dotsenko, S. Gleyzes, M. Brune, and S. Haroche, *Phys. Rev. A* **86**, 032120 (2012).
- [30] S. Haroche and J.-M. Raimond, *Exploring the Quantum. Atoms, Cavities, and Photons*. (Oxford University Press, New York, 2006).
- [31] P. Facchi and S. Pascazio, *Physical Review Letters* **89**, 080401 (2002).
- [32] P. Facchi and S. Pascazio, *Journal of Physics A* **41**, 493001 (2008).
- [33] A. Blais, R. S. Huang, A. Wallraff, S. M. Girvin, and R. J. Schoelkopf, *Physical Review A* **69**, 062320 (2004).
- [34] See Supplemental Material at ... for technical details on the protocol.
- [35] D. Kienzler, H.-Y. Lo, B. Keitch, L. de Clercq, F. Leupold, F. Lindenefelder, M. Marinelli, V. Negnevitsky, and J. P. Home, *Science* **347**, 53 (2015).
- [36] F. Schäfer, I. Herrera, S. Cherukattil, C. Lovecchio, F. S. Cataliotti, F. Caruso, and A. Smerzi, *Nature Communications* **5**, 3194 (2014).
- [37] H. P. Breuer, E. M. Laine, and J. Piilo, *Physical Review Letters* **103**, 21 (2009).
- [38] For small values of the displacement β , this choice of ϕ_z results in a quantum non-demolition measurement [41] preserving the information of the HO’s state. For $\phi_z = 2n\pi$ with odd n , corresponding to the map $|h, z\rangle \mapsto -|h, z\rangle$, the dynamics are inverted by flipping the phase of the state similar to a spin echo [42].
- [39] L. Li, M. J. Hall, and H. M. Wiseman, *Physics Reports* **759**, 1 (2018).
- [40] C. P. Koch, *J. Phys.: Condens. Matter* **28**, 213001 (2016).
- [41] G. Nogues, A. Rauschenbeutel, S. Osnaghi, M. Brune, J.-M. Raimond, and S. Haroche, *Nature* **400**, 239 (1999).
- [42] E. L. Hahn, *Phys. Rev.* **80**, 580 (1950).
- [43] S. Lorenzo, F. Plastina, and M. Paternostro, *Physical Review A* **88**, 2 (2013).
- [44] Á. Rivas, S. F. Huelga, and M. B. Plenio, *Physical Review Letters* **105**, 050403 (2010).

- [45] F. Lucas, *Adaptive resummation of Markovian quantum dynamics*, Dissertation, Universität Duisburg-Essen (2014).
- [46] P. Facchi and S. Pascazio, (2019), arXiv:1902.01591.

Implementation of the quantum simulator in cavity QED

The presented scheme is ideal for an experimental implementation in cavity QED as proposed in Ref. [29]. The harmonic oscillator can be identified by a mode of the cavity and the three-levels of the meter can be chosen to be three neighbouring circular states of the Rydberg atom, $|49C\rangle \equiv |h\rangle$, $|50C\rangle \equiv |g\rangle$, and $|51C\rangle \equiv |e\rangle$, flying through the cavity. In a fountain arrangement, the interaction time between cavity and atom is sufficiently long to perform a series of indirect measurements [29]. Due to the cryostatic environment and the long lifetime of circular states in Rydberg atoms, ‘true’ dissipation due to field energy damping or atomic relaxation is negligible on the relevant timescale. The atom will be excited to the Rydberg regime when it is already located inside the cavity which marks the beginning of one sequence of the protocol. In order to specifically address the $|h, z\rangle \leftrightarrow |+, z\rangle$ transition using the Zeno pulse Z_z and distinguish it from the nearby $|h, z\rangle \leftrightarrow |-, z\rangle$ and $|h, z\rangle \leftrightarrow |-, z-1\rangle$ transitions, the duration Δt_Z of the pulse Z has to be long enough, namely $\Delta t_Z \gg 1/(\Omega|\sqrt{z+1} - \sqrt{z}|)$ [29]. The end of one sequence with interaction time τ is triggered by ionizing the atom within the cavity by field ionization.

In the simulations presented in the main text, we take the transition frequencies of the three-level system and the HO, $\omega_{hg} = \omega'$ and $\omega_{ge} = \omega_{\text{HO}} = \omega$, and the Rabi frequency Ω from Ref. [29]. The values of ω and ω' justify the assumption of $\omega \ll \omega'$.

Identification of the optimal state pair in the non-Markovianity measure

In order to quantify memory effects, we use the BLP measure [37]. Evaluation of this measure requires comparatively little numerical effort—propagation of two well chosen initial states whereas the geometrical measure for non-Markovianity given by the state space volume [43], for instance, requires to propagate a full set of basis states. The measure proposed in [44] based on maximally entangling the system with an ancillary system leads to a further increase of the total dimension of the Hilbert space and is hence not practical for our purposes either. An obstacle for using the BLP measure is that it requires optimization over the system Hilbert space in order to identify the optimal initial state pair. On first glance, this seems difficult for the infinitely large Hilbert space of a harmonic oscillator. Nonetheless, the BLP measure turns out to be suitable in our case since we can reduce the size of the subspace in which we have to perform the optimization significantly by using our knowledge about the tailored interaction of the HO and the meter.

The reduction of the system size goes as follows, cf. Fig. 4. We know that the Zeno pulse only affects

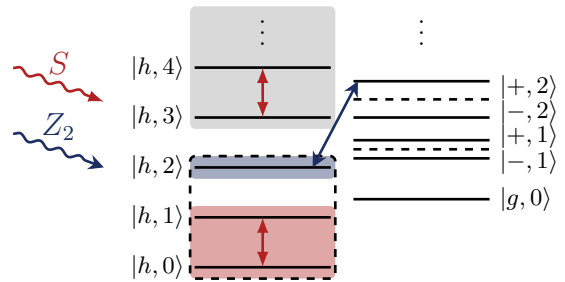


FIG. 4. Energy level diagram of the bipartite system indicating different subspaces: The Zeno subspace \mathcal{H}_Z (red shaded), the Zeno level $|z\rangle$ (blue shaded), the extended Zeno subspace \mathcal{H}_Z^+ (black dashed box) and the subspace with purely unitary dynamics (grey shaded).

the Zeno level and the level below since the dressed state we couple to is defined as $|+, z\rangle = \frac{1}{\sqrt{2}}(|e, z-1\rangle + |g, z\rangle)$. If the initial state is located within the Zeno subspace \mathcal{H}_Z , signatures of non-Markovianity can only arise from population in states within the extended Zeno subspace $\mathcal{H}_Z^+ = \{|0\rangle, \dots, |z\rangle\}$, whereas the dynamics in the remaining Hilbert space are purely unitary. Numerical tests confirm this conjecture. It is thus sufficient to consider only the extended Zeno subspace for the optimization. As in the main paper, we seek to find the optimal state pair for the special case of $z = 2$. Here, the extended Zeno subspace is only three-dimensional.

The optimization can be further simplified by considering properties of optimal state pairs for the BLP measure in general. To calculate the BLP measure, revivals of distinguishability of two initial states during a fixed time are accumulated. The distinguishability is calculated using the trace distance of the state pair at a given time. From this we can conclude that the trace distance of the optimal state pair shows revivals for the longest time with a maximal peak amplitude as compared to all other state pairs. Ideally, the states oscillate between being fully distinguishable, with trace distance equal to 1, and fully indistinguishable, with trace distance equal to 0. Thus, the dynamics of the two states which form the optimal pair should be as different from each other as possible. In our model, the Zeno level and a state within the Zeno subspace form such a pair. The former is subject to the quantum Zeno effect which means that the population in the Zeno level is frozen. For the latter, quantum Zeno dynamics (QZD) are induced and the population never leaves the Zeno subspace. Thus, in an ideal Zeno situation, this pair of initial states stays distinguishable forever. However, in our realistic model with time-resolved dynamics, the Zeno pulse introduces Rabi oscillations in the bipartite system. Thus, the overlap between the two states varies with time, leading to oscillations of the trace distance which indicate information flow and non-Markovianity. More explicitly, every

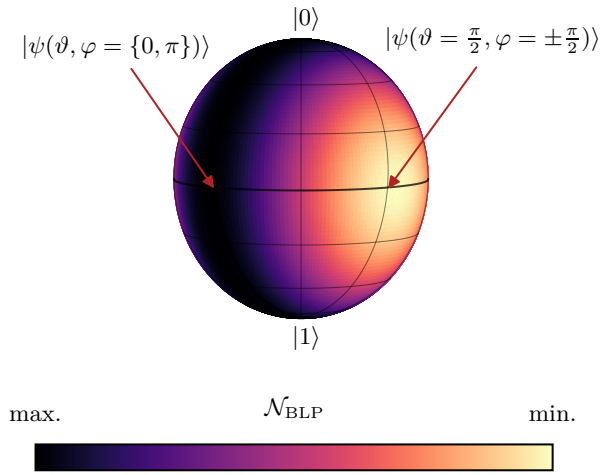


FIG. 5. BLP measure \mathcal{N}_{BLP} for different initial states $|\Psi_1\rangle = |\psi(\vartheta, \varphi)\rangle$ on the Bloch sphere spanned by the Zeno subspace $\{|0\rangle, |1\rangle\}$. The second state of the state pair is the Zeno level $|\Psi_2\rangle = |2\rangle$ outside of this subspace. The parameters are $\beta = 0.025$ and $\phi_2 = 4\pi$.

time the Zeno pulse Z_2 induces a π -pulse on the bipartite system, half of the population that has been in the Zeno level, $|h, 2\rangle$, is driven towards the level below, $|e, 1\rangle$. Thus, the distinguishability from a state within the Zeno subspace decreases. If $\phi_2 > \pi$, the population oscillates back to the state $|h, 2\rangle$, such the distinguishability increases again and the trace distance undergoes a revival. To summarize, the optimal state pair consists of the Zeno level on the one hand and a state from the Zeno subspace on the other hand.

Having reduced the optimization to an optimization over a two-dimensional space to identify the second state of the optimal pair, we proceed by parametrizing this state by its Bloch angles,

$$|\psi(\vartheta, \varphi)\rangle = \cos\left(\frac{\vartheta}{2}\right)|0\rangle + \sin\left(\frac{\vartheta}{2}\right)e^{i\varphi}|1\rangle.$$

Next, we calculate the BLP measure numerically for different initial state pairs $\{|\Psi_1\rangle = |\psi(\vartheta, \varphi)\rangle, |\Psi_2\rangle = |2\rangle\}$. The result is shown in Fig. 5. Note that the absolute value of the BLP measure has no physical meaning since it depends, amongst others but most notably, on T . It is apparent from Fig. 5 that there are several optimal state pairs, namely all states on the black circle with $\varphi = \{0, \pi\}$ and $\vartheta \in [0, \pi]$. The two states with $\varphi = \pm\frac{\pi}{2}$ and $\vartheta = \frac{\pi}{2}$ have the lowest BLP measure. This observation can be explained with the help of Fig. 6: When starting in the state $|\Psi^{\text{max}}\rangle \equiv |\psi(\vartheta = 0, \varphi = 0)\rangle = |0\rangle$ which is one of the optimal states, the population in the states $|0\rangle$ and $|1\rangle$ oscillate with α , cf. the dashed lines in Fig. 6 (top). When starting in the Zeno level $|2\rangle$, the population oscillates quickly between $|1\rangle$ and $|2\rangle$ due to the Zeno pulse (solid lines, see also the inset). The trace distance of this state pair is maximal when the first state is in $|0\rangle$ because it has no overlap with $|1\rangle$ or $|2\rangle$, seen e.g.

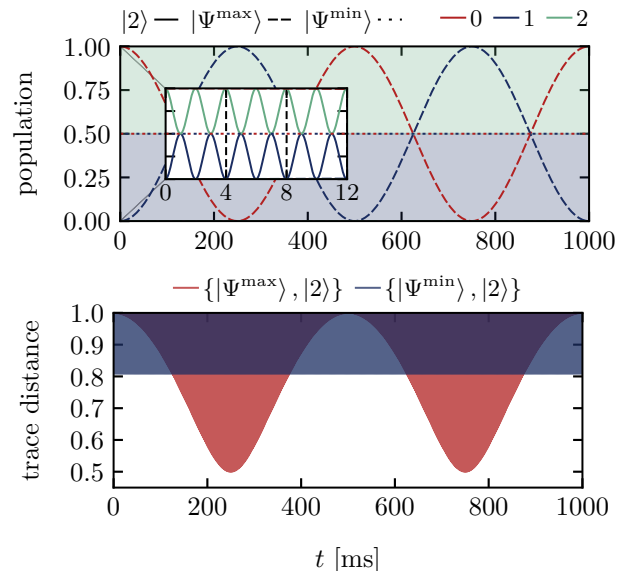


FIG. 6. Top: Evolution of the population in the Fock states with $n = 0, 1$ and 2 (red, blue and green, respectively) when starting initially in $|2\rangle$ (solid lines), $|\Psi^{\text{max}}\rangle = |0\rangle$ (dashed) and $|\Psi^{\text{min}}\rangle = \frac{1}{\sqrt{2}}(|0\rangle + i|1\rangle)$ (dotted). Note that the dotted lines for $n = 0$ and 1 are constantly equal to 0.5 . The background seems to be filled because the blue and green solid lines, corresponding to the populations in $n = 1$ and 2 when starting in $|2\rangle$, oscillate rapidly (see inset). The vertical dashed lines in the inset shows the position of the measurements. Bottom: Evolution of the trace distance for the state pairs $\{|\Psi^{\text{max}}\rangle, |2\rangle\}$ (red) and $\{|\Psi^{\text{min}}\rangle, |2\rangle\}$ (blue), respectively. The filled areas are again due to the fast oscillation. The parameters are the same as in Fig. 5.

at 0 ms in Fig. 6 (red area in the lower plot). On the other hand, the trace distance decreases to 0.5 when the first state is in $|1\rangle$ because it is, averaged over the fast oscillation, overlapping with half of the second state of the pair. Thus, the trace distance oscillates slowly with α between 0.5 and 1 , with a fast underlying oscillation with ω_Z . In contrast, $|\Psi^{\text{min}}\rangle \equiv |\psi(\vartheta = \frac{\pi}{2}, \varphi = \frac{\pi}{2})\rangle = \frac{1}{\sqrt{2}}(|0\rangle + i|1\rangle)$, which leads to the minimal BLP measure, behaves differently since it is an eigenstate of the process in the Zeno limit, cf. dotted lines in Fig. 6 (top). Thus, half of the state overlaps with the $|1\rangle$ -contribution when starting in the Zeno level all the time and the trace distance is constant with about 0.81 , with a fast underlying oscillation of the Zeno pulse, cf. Fig. 6 (blue area in the lower plot). Since the red area is larger than the blue one, the state $|\Psi^{\text{max}}\rangle$ leads to a higher BLP measure than $|\Psi^{\text{min}}\rangle$.

These observations can be easily generalized to all states on the black circle in Fig. 5 since the cavity drive S , cf. Eq. (2) in the main text, induces a rotation around the y -axis of the Bloch sphere for our choice of α . Therefore, every initial state lying on this circle will stay on it, leading to the same BLP measure for all of them. In more general terms, the rotation axis \vec{n} depends on the

phase of α via $\varphi_\alpha = \arccos\left(\frac{\text{Re}\alpha}{|\alpha|}\right)$,

$$\vec{n} = (\cos \varphi_\alpha, \sin \varphi_\alpha, 0) = (\text{Re} \alpha, \text{Im} \alpha, 0) / |\alpha|.$$

The optimal state pair is obtained when choosing $\varphi = \varphi_\alpha + \pi/2$ for the state in the Zeno subspace.

When considering two Zeno pulses, Z_1 and Z_2 , to induce non-Markovianity and dissipation, the optimal state pair is possibly different since all three states in the extended Zeno subspace \mathcal{H}_Z^\dagger take part in the non-unitary dynamics induced by the Zeno coupling and the measurement. A re-optimization was performed for the specific case of $\{\beta = 0.025, \phi_2 = 4\pi, \phi_1 = 0.25\pi\}$ providing both dissipation ($S_L = 0.48$) and a large amount of non-Markovianity (about twice as large as without having the second Zeno pulse Z_1). When optimizing $|\Psi_1\rangle$ as before, the optimal state pair for this set of parameters was found to be $\{|\Psi_1\rangle = |\psi(\vartheta = 0.56\pi, \varphi = 1.92\pi)\rangle, |\Psi_2\rangle = |2\rangle\}$. To be exact, this optimization would have to be performed for all considered parameters $\{\beta, \phi_2, \phi_1\}$ and with considering choices other than $|\Psi_1\rangle = |\psi(\vartheta, \varphi)\rangle$ and $|\Psi_2\rangle = |2\rangle$ for the optimal state pair. However, the minimal and maximal value of the BLP measure differ by about 1% only and since the absolute value of the BLP measure is not important, we choose $\{|\Psi_1\rangle = \frac{1}{\sqrt{2}}(|0\rangle + |1\rangle), |\Psi_2\rangle = |2\rangle\}$ throughout for simplicity.

Derivation of the Lindblad master equation

We now provide the detailed derivation of the Lindblad master equation (6) starting from the piecewise dynamics of Eq. (4). The first step is to evaluate the partial trace and to derive the Krauss representation of the map. To this end, we have to expand the time evolution operator $\hat{U}(dt)$ using the Baker-Campbell-Hausdorff formula up to first order,

$$\begin{aligned} \hat{U}(dt) &= e^{-i(\hat{H}_{CS} + \hat{H}_{AC} + \hat{H}_Z)dt} \\ &\approx e^{-i\hat{H}_Z dt} e^{-i\hat{H}_{CS} dt} e^{-i\hat{H}_{AC} dt} \end{aligned}$$

Using $[\hat{H}_{AC}, |h\rangle\langle h|] = 0$ and the fact that we start each sequence with the initial state $\hat{\rho}(t) = \hat{\rho}_C(t) \otimes |h\rangle\langle h|$, we can evaluate the partial trace explicitly. We arrive at

$$\hat{\rho}_C(t+dt) = \sum_{j=h,g,e} w_{jh} \hat{U}_{CS}(dt) \hat{\rho}_C(t) \hat{U}_{CS}^\dagger(dt) w_{jh}^\dagger \quad (8)$$

with $\hat{U}_{CS}(dt) = e^{-i\hat{H}_{CS} dt}$ and $w_{jh} = \langle j | \hat{U}_Z(dt) | h \rangle$ with $\hat{U}_Z(dt) = e^{-i\hat{H}_Z dt}$. Diagonalisation of $\hat{U}_Z(dt)$ leads to [29]

$$\hat{U}_Z(dt) = e^{-i\frac{\phi_z}{2} \hat{P}_+} + e^{i\frac{\phi_z}{2} \hat{P}_-} + \hat{P}_\perp$$

with the Rabi angle $\phi_z = \omega_Z dt$, the projectors $\hat{P}_\pm = |u_\pm\rangle\langle u_\pm|$, $\hat{P}_\perp = \hat{1} - \hat{P}_+ - \hat{P}_-$ and the states $|u_\pm\rangle = \frac{1}{\sqrt{2}}(|h, z\rangle \pm |+, z\rangle)$. This expression can be used to evaluate the operators w_{jh} ,

$$w_{hh} = \hat{1}_C - \left(1 - \cos \frac{\phi_z}{2}\right) \hat{\Pi}, \quad (9a)$$

$$w_{gh} = \frac{1}{\sqrt{2}} \sin \frac{\phi_z}{2} \hat{\Pi}, \quad (9b)$$

$$w_{eh} = \frac{1}{\sqrt{2}} \sin \frac{\phi_z}{2} \hat{A}, \quad (9c)$$

where $\hat{\Pi}$ and \hat{A} are photonic operators, $\hat{\Pi} = |z\rangle\langle z|$ and $\hat{A} = |z-1\rangle\langle z|$. Note that Eq. (8) can be interpreted both as the description of a measurement process with three measurement operators and as the Krauss representation of the evolution of an open quantum system.

Furthermore, a time-continuous master equation in Lindblad form can be derived by assuming the measurement to be performed continuously with constant rate $\kappa = \frac{1}{\tau}$ such that the number of measurements in a time interval dt is κdt . This can be interpreted as ‘‘smearing’’ of one measurement over the whole time interval τ . As a result, the master equation will not describe the same evolution as the piecewise dynamics for large values of τ . Using this assumption and going to the interaction picture with respect to the coherent evolution \hat{H}_{CS} , we can rewrite Eq. (8) to [45]

$$\hat{\rho}_C(t+dt) = \kappa dt \sum_{j=h,g,e} w_{jh} \hat{\rho}_C(t) w_{jh}^\dagger + (1 - \kappa dt) \hat{\rho}_C(t).$$

Finally, we calculate the derivative of the reduced state as $\frac{d\hat{\rho}_C(t)}{dt} = \lim_{dt \rightarrow 0} \frac{\hat{\rho}_C(t+dt) - \hat{\rho}_C(t)}{dt}$ and go back to the non-interacting picture [45],

$$\begin{aligned} \frac{d\hat{\rho}_C(t)}{dt} &= -i \left[\hat{H}_{CS}, \hat{\rho}_C \right] \\ &+ \kappa \left(\sum_{j=h,g,e} w_{jh} \hat{\rho}_C(t) w_{jh}^\dagger - \hat{\rho}_C(t) \right). \end{aligned}$$

After inserting the Krauss operators of Eq. (9) and rearranging the terms using that $\hat{\Pi}$ is idempotent and $\hat{\Pi} = \hat{A}^\dagger \hat{A}$, we arrive at the master equation as shown in Eq. (6).

To assess the agreement of the master equation (6) with the piecewise dynamics of Eq. (4), we propagate the initial state $|0\rangle$ with $z = 2$ using both methods. Fig. 7 shows the difference in infidelity of the QZD, $P_{\bar{Z}}$, and in the linear entropy S_L between the two pictures. It can be seen that they show good agreement for small Rabi angles ϕ_2 or displacements β . However, the two pictures deviate when our assumptions during the derivation of the master equation are violated. Firstly, the agreement deteriorates for large β , since this contradicts the assumption of continuous measurements, $dt \rightarrow 0$. Secondly, we have used the Baker-Campbell-Hausdorff formula up to

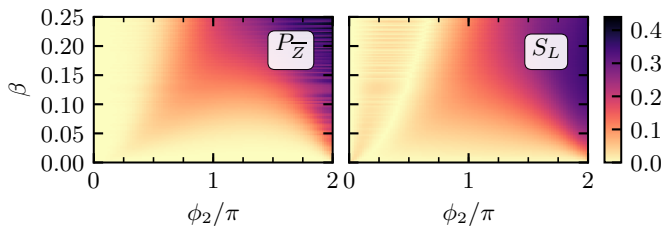


FIG. 7. Difference obtained when solving the master equation and using the piecewise dynamics for the Zeno infidelity P_Z (left) and the dissipation S_L (right) as a function of the displacement β due to the classical drive S and the Rabi angle ϕ_2 accumulated due to the Zeno pulse Z_2 .

first order to derive the Krauss representation. We thus make an error which is of the order of the commutator of \hat{H}_S and \hat{H}_z which scales as $\phi_z\beta$. Therefore, the deviation also gets larger as ϕ_2 increases.

Effects leading to Zeno confinement

Quantum Zeno dynamics describe the effect of confining the dynamics of a system to a tailored subspace by frequent measurements. The dynamics shown in Fig. 2 and 7 agree with this intuitive picture since the Zeno infidelity vanishes as the displacement β , which is proportional to the time inbetween two measurements, goes to zero. However, Zeno confinement occurs also in other regions as will be explained in the following.

(i) QZD can not only be induced by frequent measurements but also by strongly coupling the system to a meter. In fact, the two cases are formally equivalent in the limit of a fast repetition rate and strong coupling [46]. In our case, the strength of the coupling between the HO and the three-level system is given by the field strength

of the Zeno pulse, $\omega_z = \phi_z/\tau$, which is proportional to the Rabi angle ϕ_z . Thus, the quality of the Zeno confinement is very good for large values of the Rabi angle ϕ_z even if β is large.

(ii) The coupling of the Zeno level to the dressed state $|+, z\rangle$ induces a decay of the Zeno level's population to the level below. This can be explained by considering the piecewise dynamics of Eq. (4) and the effect of the Zeno pulse Z_z . If the initial state $|h, z\rangle$ is evolved under the action of the Hamiltonian \hat{H}_z in Eq. (3) (while neglecting the action of the source S), the atom-field state at time τ is given by

$$|\Psi_{|h,z\rangle}(\tau)\rangle = \cos\left(\frac{\phi_z}{2}\right)|h, z\rangle + \sin\left(\frac{\phi_z}{2}\right)|+, z\rangle, \quad (10)$$

where $\phi_z = \omega_z\tau$ is the Rabi angle. All other states $|h, n \neq z\rangle$ are unaffected by \hat{H}_z . It can be seen that, when performing a Zeno pulse with Rabi angle $\phi_z \neq 2n\pi$, a fraction of $\sin^2\left(\frac{\phi_z}{2}\right)$ of the population that has been in the state $|h, z\rangle$ ends up in the state $|+, z\rangle$. According to the definition of the dressed states, half of the photons are in the state $|z-1\rangle$ here, i.e. back in the Zeno subspace, which enhances the Zeno confinement. In the Lindblad master equation 6, the same effect is achieved by the Lindblad operator \hat{A} as can be seen from the reappearing $\sin^2\left(\frac{\phi_z}{2}\right)$ -contribution in the decay rate γ_A . As a consequence, if the initial state is lying above the Zeno level, $n_0 > z$, the Zeno pulse has to be changed to be resonant to the $|h, z\rangle \leftrightarrow |+, z+1\rangle$ transition, to also benefit from this enhancement.

(iii) For $\pi < \phi_z < 2\pi$, the phase of the $|h, z\rangle$ contribution in Eq. (10) is negative due to the cosine. This leads to an inversion of the dynamics back into the Zeno subspace which improves the QZD additionally.